

X-RAY SPECTROSCOPY OF THE LOW-MASS X-RAY BINARIES 2S 0918–549 AND 4U 1543–624:  
EVIDENCE FOR NEON-RICH DONORSADRIENNE M. JUETT AND DEEPTO CHAKRABARTY<sup>1</sup>Department of Physics and Center for Space Research, Massachusetts Institute of Technology, Cambridge, MA 02139;  
ajuett, deepto@space.mit.edu*Accepted for publication in the Astrophysical Journal*

## ABSTRACT

We present high-resolution spectroscopy of the neutron-star/low-mass X-ray binaries 2S 0918–549 and 4U 1543–624 with the High Energy Transmission Grating Spectrometer onboard the *Chandra X-ray Observatory* and the Reflection Grating Spectrometer onboard *XMM-Newton*. Previous low-resolution spectra of both sources showed a broad line-like feature at 0.7 keV that was originally attributed to unresolved line emission. We recently showed that this feature could also be due to excess neutral Ne absorption, and this is confirmed by the new high-resolution *Chandra* spectra. The *Chandra* spectra are each well fit by an absorbed power-law + blackbody model with a modified Ne/O number ratio of  $0.52 \pm 0.12$  for 2S 0918–549 and  $1.5 \pm 0.3$  for 4U 1543–624, compared to the interstellar-medium value of 0.18. The *XMM* spectrum of 2S 0918–549 is best fit by an absorbed power-law model with a Ne/O number ratio of  $0.46 \pm 0.03$ , consistent with the *Chandra* result. On the other hand, the *XMM* spectrum of 4U 1543–624 is softer and less luminous than the *Chandra* spectrum and has a best-fit Ne/O number ratio of  $0.54 \pm 0.03$ . The difference between the measured abundances and the expected interstellar ratio, as well as the variation of the column densities of O and Ne in 4U 1543–624, supports the suggestion that there is absorption local to these binaries. We propose that the variations in the O and Ne column densities of 4U 1543–624 are caused by changes in the ionization structure of the local absorbing material. It is important to understand the effect of ionization on the measured absorption columns before the abundance of the local material can be determined. This work supports our earlier suggestion that 2S 0918–549 and 4U 1543–624 are ultracompact binaries with Ne-rich companions.

*Subject headings:* binaries: close — stars: neutron — stars: individual (2S 0918–549) — stars: individual (4U 1543–624) — X-rays: binaries

## 1. INTRODUCTION

Low mass X-ray binaries (LMXBs) consist of a neutron star (NS) or black hole (BH) in orbit with a  $\lesssim 1 M_{\odot}$  companion. An intriguing sub-class of LMXBs are the ultracompact binaries that have orbital periods less than 80 minutes. Hydrogen-rich companions cannot sustain a LMXB system with such a short orbital period (Paczynski & Sienkiewicz 1981; Rappaport, Joss, & Webbink 1982). However, orbital periods  $\lesssim 80$  min are predicted for hydrogen-deficient or degenerate companions (Joss, Avni, & Rappaport 1978; Nelson, Rappaport, & Joss 1986), and this was confirmed with the orbital period measurements of the X-ray pulsar 4U 1626–67 ( $P_{\text{orb}}=42$  min; Middleditch et al. 1981), the X-ray dipper 4U 1915–05 ( $P_{\text{orb}}=50$  min; White & Swank 1982; Walter et al. 1982), the X-ray bursters 4U 1820–30 ( $P_{\text{orb}}=11$  min; Stella, Priedhorsky, & White 1987) and 4U 1850–087 ( $P_{\text{orb}}=21$  min; Homer et al. 1996), and the detection of the white dwarf analogs, the AM CVn systems (e.g., Warner 1995). In addition, the three recently discovered millisecond X-ray pulsars XTE J1751–305, XTE J0929–314, and XTE J1807–294 were also found to be ultracompact binaries with  $P_{\text{orb}} = 42, 44$ , and 35 min, respectively (Markwardt et al. 2002; Galloway et al. 2002; Markwardt, Smith, & Swank 2003). The conventional wisdom has been that the companions in ultracompact

LMXBs are the remains of He white dwarfs (WDs) that have transferred a significant fraction of their mass to the NS. However, recent X-ray spectral evidence indicates that some companions may be Ne-rich (Schulz et al. 2001; Juett, Psaltis, & Chakrabarty 2001), which suggests the possibility of C-O or O-Ne-Mg WD companions. The growing population of these exotic ultracompact systems, as well as the new evidence for Ne-rich companions, has interesting implications for the formation and evolution of binary systems. Motivated by the observational evidence for Ne-rich donors, Yungelson, Nelemans, & van den Heuvel (2002) explored formation scenarios for these systems. Here we discuss two other NS/LMXBs that may also be ultracompact binaries.

Both 2S 0918–549 ( $l = 275.9^\circ$ ,  $b = -3.8^\circ$ ) and 4U 1543–624 ( $l = 321.8^\circ$ ,  $b = -6.3^\circ$ ) have been observed by all of the major X-ray satellites since *Uhuru*. McClintock et al. (1978) identified the optical counterpart of 4U 1543–624 based on the *SAS-3* position, which was confirmed by *HEAO 1*. The flux measurements of 4U 1543–624 are roughly constant over the last 25 years (Singh, Apparao, & Kraft 1994; Christian & Swank 1997; Asai et al. 2000; Juett et al. 2001; Schultz 2002; Farinelli et al. 2003) with no periodicities from 50 s – 10,000 s found in the *EXOSAT* data, and no periodicities from 0.1 s – 1000 s detected in the *SAX* data. Recently, Schultz (2002) presented spectral results from archival *ASCA*, *SAX*, and *RXTE* ob-

<sup>1</sup> Alfred P. Sloan Research Fellow

servations. These results suggest that an increase in the luminosity of 4U 1543–624 is accompanied by a hardening of the spectrum. In addition, an Fe-K emission line is seen in the hard state, but not detected in the low state. Farinelli et al. (2003) present an independent analysis of the two *SAX* observations which show no significant luminosity change but a spectral hardening in the second observation. Both Farinelli et al. (2003) and Asai et al. (2000) report Fe-K line detections for the *SAX* and *ASCA* observations, respectively.

In contrast, 2S 0918–549 shows a factor of 10 X-ray variability, but again has no known periodicities in either the X-ray or optical bands down to timescales of 1 hour (Forman et al. 1978; Warwick et al. 1981; Chevalier & Ilovaisky 1987; Smale & Lochner 1992; Christian & Swank 1997; Schulz 1999; Jonker et al. 2001). Chevalier & Ilovaisky (1987), using the *Einstein* HRI position, identified an ultraviolet-bright optical counterpart for 2S 0918–549 and suggested a source distance of 15 kpc based on the properties of other LMXBs, i.e.,  $M_V=0.0$  and  $(B-V)_0=0.0$ . Recently, Jonker et al. (2001) detected a type I X-ray burst from 2S 0918–549 and derived an upper limit to the distance of 4.9 kpc from radius expansion arguments. A similar analysis using *BepoSAX* Wide Field Camera data of 2S 0918–549 implied a distance of 4.2 kpc (Cornelisse et al. 2002).

We have identified both 2S 0918–549 and 4U 1543–624 as being part of a class of four NS/LMXBs all having a similar feature at 0.7 keV in their low-resolution spectra (Juett et al. 2001). This feature had been attributed to unresolved line emission from Fe and O (see, e.g., Christian, White & Swank 1994; White, Kallman & Angelini 1997). However, a high-resolution observation of the brightest of these sources, 4U 0614+091, with the *Chandra X-Ray Observatory*, failed to detect any emission lines, finding instead an unusually high Ne/O number ratio in the absorption along the line of sight (Paerels et al. 2001). Previously, we showed that the *ASCA* spectra of all four sources are well fit *without* a 0.7 keV emission line using a model that includes photoelectric absorption due to excess Ne along the lines of sight and presumably local to the sources. In this paper, we present the high-resolution *Chandra* and *XMM-Newton* spectra of two sources, 2S 0918–549 and 4U 1543–624, which support our earlier *ASCA* results.

Given the high  $L_X/L_{\text{opt}}$  ratio of these sources and the excess Ne absorption, we suggested that the systems are ultracompact binaries with Ne-rich degenerate donors (Juett et al. 2001). This is similar to the ultracompact X-ray pulsar 4U 1626–67. We note that while the spectrum of 4U 1626–67 does show O and Ne emission lines (Angelini et al. 1995; Schulz et al. 2001), it does not resemble the sources we are considering in either low or high-resolution spectra. While we do compare our results to those of 4U 1626–67, it is important to consider the differences between the systems when drawing conclusions.

## 2. OBSERVATIONS AND DATA REDUCTION

*Chandra* observed 2S 0918–549 on 2000 July 19 and 4U 1543–624 on 2000 September 12 for 30 ks each using the High Energy Transmission Grating Spectrometer (HETGS) and the Advanced CCD Imaging Spectrome-

ter (ACIS; Weisskopf et al. 2002). The HETGS carries two transmission gratings: the Medium Energy Gratings (MEGs) with a range of 2.5–31 Å (0.4–5.0 keV) and the High Energy Gratings (HEGs) with a range of 1.2–15 Å (0.8–10.0 keV). The HETGS spectra are imaged by ACIS, an array of six CCD detectors. The HETGS/ACIS combination provides both an undispersed (zeroth order) image and dispersed spectra from the gratings. The various orders overlap and are sorted using the intrinsic energy resolution of the ACIS CCDs. The first-order MEG (HEG) spectrum has a spectral resolution of  $\Delta\lambda = 0.023$  Å (0.012 Å).

The “level 1” event files were processed using the CIAO v2.2 data analysis package. For both sources, the standard CIAO spectral reduction procedure was performed. During our analysis, it was found that the pipeline tool `acis_detect_afterglow` rejects 3–5% of source photons in grating spectra. Afterglow is the residual charge left from a cosmic-ray event which is released over several frames and can cause a line-like feature in a grating spectrum. The `acis_detect_afterglow` tool flags events that occur at the same chip coordinates in consecutive frames. For bright sources, the tool also rejects a fraction of the source events. Although only a small fraction of the total, the rejection of source photons by this tool is systematic and non-uniform. Since order-sorting of grating spectra provides efficient rejection of background events, the afterglow detection tool is not necessary. Therefore, we reextracted the event file, retaining those events tagged by the `acis_detect_afterglow` tool. No features were found that might be attributable to afterglow events.

The combined MEG + HEG first order dispersed spectrum of 2S 0918–549 has an average count rate of  $3.10 \pm 0.18$  cts s<sup>-1</sup>. We examined the total count rate, as well as the count rates in three different energy ranges, to check for changes in the spectral state of 2S 0918–549. We found no evidence for any change of state during the *Chandra* observation. For 4U 1543–624, the first order MEG + HEG count rate is  $17.2 \pm 0.4$  cts s<sup>-1</sup>. Similarly, no changes of state of 4U 1543–624 were found. To look for periodic modulations of the X-ray flux, we created lightcurves from the combined first order event files after barycentering and randomizing the event arrival times. Randomizing of the event arrival times consists of adding a random quantity uniformly distributed between 0–3.2 s in order to avoid aliasing caused by the readout time. We searched for modulations of the X-ray flux with frequencies between  $4 \times 10^{-5}$  and  $5 \times 10^{-2}$  Hz. We found no evidence for periodic modulation in either source, with a 90%-confidence upper limit of 2% (2S 0918–549) and 1% (4U 1543–624) for the fractional rms amplitude.

For both observations, we applied the aspect offset correction available at the *Chandra* website<sup>2</sup>. Using the CIAO tool `celldetect`, the zeroth order source position for 2S 0918–549 was determined: R.A.=09<sup>h</sup>20<sup>m</sup>26<sup>s</sup>.95 and Dec=−55°12'24".7, equinox J2000.0 (90% confidence error of 0''.6). Since the optical counterpart position is not given by Chevalier & Ilovaisky (1987), we obtained optical images of the 2S 0918–549 field using the Magellan 6.5-m telescopes in Chile. We measured the position of the optical counterpart by

<sup>2</sup> See <http://asc.harvard.edu/cal/ASPECT/celmon/index.html>

matching about 20 field stars with the USNO-A2.0 catalog of astrometric standards (Monet et al. 1998). We obtained R.A.=09<sup>h</sup>20<sup>m</sup>26<sup>s</sup>.99 and Dec=−55°12'24".8 (equinox J2000.0) with an error radius of 1".8 (90% confidence). The optical and X-ray positions for 2S 0918−549 are 1".5 separated. The zeroth order image of 4U 1543−624 was so heavily piled up that no counts were recorded in the center of the point spread function. `Celldetect` was not able to determine an accurate source position, but the CIAO tool `tgdetect`, which runs `celldetect` in conjunction with grating specific filters and sub-tools, was able to position the zeroth order image of 4U 1543−624: R.A.=15<sup>h</sup>47<sup>m</sup>54<sup>s</sup>.69 and Dec=−62°34'05".4, equinox J2000.0. This position is 0".2 from the optical counterpart position given by Bradt & McClintock (1983).

For bright sources, pileup can be a problem for CCD detectors (see, e.g., Davis 2003). Pileup occurs when two or more photons are incident on the same pixel during the 3.2 s readout time of the ACIS detector. When this happens, the instrument reads just one event at an energy comparable to the sum of the original photons energies, thus reducing the detected count rate and modifying the spectral shape. The zeroth order *Chandra* spectra of both 2S 0918−549 and 4U 1543−624 were heavily affected by pileup (pileup fraction >80%) and were not used in this analysis. In addition, pileup can also affect dispersed spectra. We checked the dispersed spectra of both sources and found that for 2S 0918−549 no pileup occurred; whereas for 4U 1543−624, there were signs of pileup in the first order MEG spectrum. In dispersed spectra, pileup can affect only a limited wavelength range, particularly where the effective area of the instrument is the highest. For 4U 1543−624, pileup occurred in the range 5–12 Å (1–2.5 keV).

For 2S 0918−549, we used the standard CIAO tools to create detector response files (ARFs) for the MEG and HEG +1 and −1 order spectra. These were combined when the +/− order spectra were added for the MEG and HEG separately. The data were binned to 0.03 Å (0.015 Å) for the MEG (HEG) to ensure good statistics. We also created background files for the MEG and HEG spectra using the standard CIAO tool.

There are known differences in the quantum efficiencies (QEs) of the front-illuminated (FI) CCDs compared to the back-illuminated (BI) CCDs. An initial analysis using the standard QE files revealed that, for 4U 1543−624, the chip differences were identifiable (especially at high wavelengths) and needed to be corrected. Using a correction table<sup>3</sup> provided by H. L. Marshall of the HETGS instrument team, we modified the QE files available in the standard CIAO calibration database and then used them to create ARFs for the spectral analysis of 4U 1543−624. This modification was not required for the 2S 0918−549 data. In order to use the grating pileup kernel in ISIS, we created ARFs for each chip using the CIAO tool `mkgarf` and then combined them to create +1 and −1 order MEG and HEG ARFs using a custom tool developed by J. Davis of the HETGS instrument team. (This tool is similar to the standard CIAO tool but also correctly calculates the fractional exposure at each response bin.

This functionality has been added to the standard tools in CIAO v2.3.) The grating pileup kernel models the effect of pileup on grating spectra, similar to the pileup model available for CCD spectra in ISIS and XSPEC (see, Davis 2003, for a discussion of grating pileup modeling). In addition, the data and responses were rebinned to 0.033 Å (0.017 Å) for the MEG (HEG) to reflect the size of an ACIS event detection cell (3 CCD pixels). We used this binning for the spectral analysis. All *Chandra* spectral analysis of 2S 0918−549 and 4U 1543−624 was performed using ISIS (Houck & DeNicola 2000).

*XMM* observed 2S 0918−549 on 2001 May 5 for 40 ks and 4U 1543−624 on 2001 Feb 4 for 50 ks. *XMM* carries three different instruments, the European Photon Imaging Cameras (EPICs; Strüder et al. 2001; Turner et al. 2001) the Reflection Grating Spectrometers (RGSs; den Herder et al. 2001), and the Optical Monitor (OM; Mason et al. 2001). The OM was not used in this analysis.

The EPIC instruments consist of 3 CCD cameras, MOS 1, MOS 2, and pn, which provide imaging, spectral and timing data. For both observations, the pn and MOS 1 cameras were run in timing mode which provides high time resolution event information by sacrificing 1-dimension in positional information. During the 2S 0918−549 observation, the MOS 2 camera was run in full-frame mode, while for the 4U 1543−624 observation, it was run in small-window mode. The EPIC instruments provide good spectral resolution ( $\Delta E=50$ –200 eV FWHM) over the 0.3–12.0 keV range. There are two RGSs onboard *XMM* which provide high-resolution spectra ( $\lambda/\Delta\lambda=100$ –500 FWHM) over the 5–38 Å range. The grating spectra are imaged onto CCD cameras similar to the EPIC-MOS cameras which allows for order sorting of the high-resolution spectra.

The *XMM* data were reduced using SAS version 5.3. Standard filters were applied to all *XMM* data and times of high background were excluded. The EPIC-pn data were reduced using the procedure `epchain`. Source and background spectra were extracted using filters in the one spatial coordinate, DETX. A ready-made response file for pn timing mode data can be found on the *XMM* website<sup>4</sup>. We reduced the EPIC-MOS data using `emchain`. Since no response file was available for MOS timing mode observations, the MOS 1 data were not used in this analysis. The MOS 2 data were found to have considerable pileup. To reduce the effect of pileup on the spectra, we extracted source spectra using an annulus to excise the core of the point spread function where pileup is prevalent. The inner 20" were excluded for 2S 0918−549 and the inner 35" for 4U 1543−624. Background spectra were extracted using an annulus centered on the source but excluding any other point sources in the field of view. Response files were generated for the MOS 2 spectra using `rmfgen` and `arfgen`. The RGS data were reduced using `rgsproc`, which produced standard first order source and background spectra and response files for both RGSs. We grouped the pn and MOS spectra to oversample the energy resolution of the CCDs by no more than a factor of three. The RGS spectra were grouped to ensure that each bin had at least 20 counts. All *XMM* spectral analysis of 2S 0918−549 and 4U 1543−624 was performed

<sup>3</sup> Documentation and table available at <http://space.mit.edu/CXC/calib/hetgcal.html>

<sup>4</sup> Available at <http://xmm.vilspa.esa.es/ccf/epic/>

using XSPEC (Arnaud 1996).

The 2S 0918–549 observation had average count rates of  $81.06 \pm 0.05$ ,  $13.03 \pm 0.02$ , and  $8.928 \pm 0.016$  cts s $^{-1}$  for the pn, MOS 2, and combined RGS, respectively. Using the pn data, we checked for changes in the spectral state by examining the total count rate, as well as the count rates in three different energy ranges. There was no evidence for a change in the spectral state of 2S 0918–549 during the *XMM* observation. The average count rates during the 4U 1543–624 observation were  $238.89 \pm 0.07$ ,  $46.88 \pm 0.03$ , and  $23.07 \pm 0.02$  cts s $^{-1}$  for the pn, MOS 2, and combined RGS, respectively. Again, no change in the spectral state of 4U 1543–624 was found during the *XMM* observation. While the pn timing mode allows for a time resolution of 0.03 ms, searches for periodic and quasi-periodic modulation at high frequency are hampered by a 167 Hz instrumental signal (and multiple harmonics). Due to the low count rates of these observations ( $\ll 1$  count per readout), the low frequency end of the power spectrum is affected by instrumental noise (see, Kuster et al. 2002, and references therein). To remove the noise, we calculated the average power at each frequency using an 11 bin moving average and then divided by this value. We verified that the powers were distributed correctly and then searched for modulation of the X-ray flux with frequencies between  $2 \times 10^{-5}$  and 0.5 Hz. No modulation was detected with a 90%-confidence upper limit on the fractional rms amplitude of 0.3% (2S 0918–549) and 0.14% (4U 1543–624).

### 3. SPECTRAL RESULTS

#### 3.1. 2S 0918–549

To determine the appropriate continuum model, we fit the *Chandra* HEG and MEG spectra jointly with both an absorbed power-law and an absorbed power-law + blackbody model over the wavelength ranges 1.5–13 Å for the HEG and 1.8–25 Å for the MEG. In all cases, we used the interstellar absorption model of Wilms, Allen, & McCray (**tbabs**; 2000). In addition, we included an edge at 43.7 Å to account for the instrumental C buildup on the ACIS CCDs<sup>5</sup> (Plucinsky et al. 2002). We calculated that the appropriate optical depth for the instrumental C edge at the time of the 2S 0918–549 observation was 0.79 from calibration data points provided by H. L. Marshall. This edge is included in all *Chandra* spectral fits of 2S 0918–549. The power-law + blackbody model produced a significantly better chi-squared value than the power-law alone (significance greater than 99.99% as calculated by an F-test), so we take a power-law + blackbody model as the appropriate continuum model for the *Chandra* spectra. The best-fit parameter values are given in Table 1.

We showed that the lower-resolution *ASCA* spectra of 2S 0918–549 could be well fit by including photoelectric absorption with non-solar abundances of O and Ne (Juett et al. 2001). High-resolution spectroscopy can test the accuracy of this hypothesis by directly measuring the edge depths, and therefore column densities, of neutral O, Fe, and Ne. We can then compare the abundance ratios to those expected for the interstellar medium (ISM). To determine the columns of each of

these elements, we replaced the absorption model with the comparable variable abundance absorption model (**tbvarabs**; Wilms et al. 2000) and set the abundances of O, Fe and Ne to zero. The  $N_{\text{H}}$  parameter was allowed to vary while all other absorption model parameters were frozen. The Ne and O-K edges were each modeled by a multiplicative edge model of the form:

$$M(E) = \begin{cases} 1 & \text{for } E < E_{\text{edge}}, \\ \exp[-\tau(E/E_{\text{edge}})^{-3}] & \text{for } E \geq E_{\text{edge}}, \end{cases} \quad (1)$$

with  $\tau$  and  $E_{\text{edge}}$  as variable parameters. Individual edge models are used since the edge positions and shapes in the standard absorption models are not appropriate for high-resolution spectral analysis (see, Wilms et al. 2000; Juett et al. 2003, in preparation). A Gaussian line was included to model the interstellar absorption line due to atomic O at 23.5 Å. The more complex Fe-L edge at 17.5 Å was modeled using a table model, created from the optical constant measurements by Kortright & Kim (2000), which allowed for both the column density of Fe and the edge energy to vary. The continuum was again described by a power law + blackbody. The resulting parameters for the power-law and blackbody models are consistent with the low-resolution fit. The results of the fit can be found in Table 1 and are shown in Figure 1.

From the absorption edge depths, the absorbing column densities of O, Fe, and Ne can be determined along with the equivalent hydrogen column for each element assuming interstellar abundances. These results are summarized in Table 2. The atomic cross-sections of Henke, Gullikson, & Davis (1993) were used for O and Ne, while the Fe-L cross-section was taken from Kortright & Kim (2000). We use the ISM abundances given by Wilms et al. (2000) to calculate equivalent hydrogen column densities. The wavelengths of the edges are consistent with measurements of neutral ISM edges in other LMXBs (Juett et al. 2003). We find a Ne column density of  $N_{\text{Ne}} = (9.9 \pm 1.7) \times 10^{17}$  cm $^{-2}$  and an O column density of  $N_{\text{O}} = (1.9 \pm 0.3) \times 10^{18}$  cm $^{-2}$  (all errors quoted at 90%-confidence level). The equivalent hydrogen column implied by the Ne edge is roughly three times that calculated from the O edge. We find a Ne/O number ratio of  $0.52 \pm 0.12$ , compared to the ISM ratio of 0.18. The measured Fe column is  $N_{\text{Fe}} = (10^{+6}_{-3}) \times 10^{16}$  cm $^{-2}$ . The atomic O absorption line has a wavelength of  $23.52 \pm 0.04$  Å and an equivalent width (EW) of  $0.017 \pm 0.010$  Å.

The evidence for Ne enhancement in the absorption to 2S 0918–549 is similar to what is seen in 4U 1626–67 (Schulz et al. 2001). Since the spectrum of 4U 1626–67 also shows emission lines from Ne and O, we performed a careful search of the *Chandra* spectral residuals of 2S 0918–549 to place limits on the presence of any spectral line features. Gaussian models with fixed FWHM=2000 km s $^{-1}$  were fit at each point in the wavelength range 1.5–13 Å for the HEG and 1.8–25 Å for the MEG. From this, we can place a  $3\sigma$  upper limit on the EW of any line feature, either emission or absorption. The EW limit increases with wavelength, varying from 0.02 Å at 1.5 Å to 0.5 Å at 23 Å. These EW limits are 3–10 times lower than the line EWs found in the *Chandra* observation of 4U 1626–67. Since the lines found in the spectrum of 4U 1626–67 were broader, FWHM of

<sup>5</sup> For more information see, [http://cxc.harvard.edu/cal/Links/Acis/acis/Cal\\_prods/qeDeg/index.htm](http://cxc.harvard.edu/cal/Links/Acis/acis/Cal_prods/qeDeg/index.htm)

TABLE 1. SPECTRAL FITS<sup>a</sup>

Model <sup>b</sup>	Absorption		Power-law		Blackbody		$\chi^2/\text{dof}$
	$N_{\text{H}}$ ( $10^{21} \text{ cm}^{-2}$ )	$\Gamma$	$A_1^c$	$kT$ (keV)	$R_{\text{km}}^2/d_{10\text{kpc}}^2$		
2S 0918–549							
<i>Chandra</i> tbabs×(PL+BB)	2.4±0.3	2.04±0.08	2.9±0.3	0.54±0.02	30±9	1.11	
<i>Chandra</i> full model	2.9±0.3	2.10±0.09	3.3±0.5	0.55±0.04	23±9	1.07	
<i>XMM</i> tbabs×PL	2.95±0.02	2.265±0.004	6.23±0.03	...	...	1.61	
<i>XMM</i> full model	3.20±0.03	2.25(fixed)	5.48±0.06	...	...	1.27	
4U 1543–624							
<i>Chandra</i> tbabs×(PL+BB)	1.58±0.11	1.539 <sup>+0.03</sup> <sub>-0.004</sub>	12.6±0.6	0.62±0.03	61±13	1.75	
<i>Chandra</i> full model	3.31±0.014	1.97(fixed)	17.1±0.8	...	...	1.32	
<i>XMM</i> tbabs×(PL+BB)	3.478±0.017	2.568±0.008	25.12±0.11	1.480±0.005	3.38±0.07	4.34	
<i>XMM</i> full model	3.613±0.014	2.7(fixed)	16.26±0.06	1.512(fixed)	18.5±0.3	1.87	

<sup>a</sup>All errors are quoted at the 90%-confidence level

<sup>b</sup>PL=power law; BB=blackbody; tbabs=photoelectric absorption model of Wilms et al. (2000); full model=absorption of O, Fe, and Ne modeled by edge models with O absorption lines where needed. The results for the edge models are given in Table 2.

<sup>c</sup>Power-law normalization at 1 keV in units of  $10^{-2}$  photons  $\text{keV}^{-1} \text{ cm}^{-2} \text{ s}^{-1}$

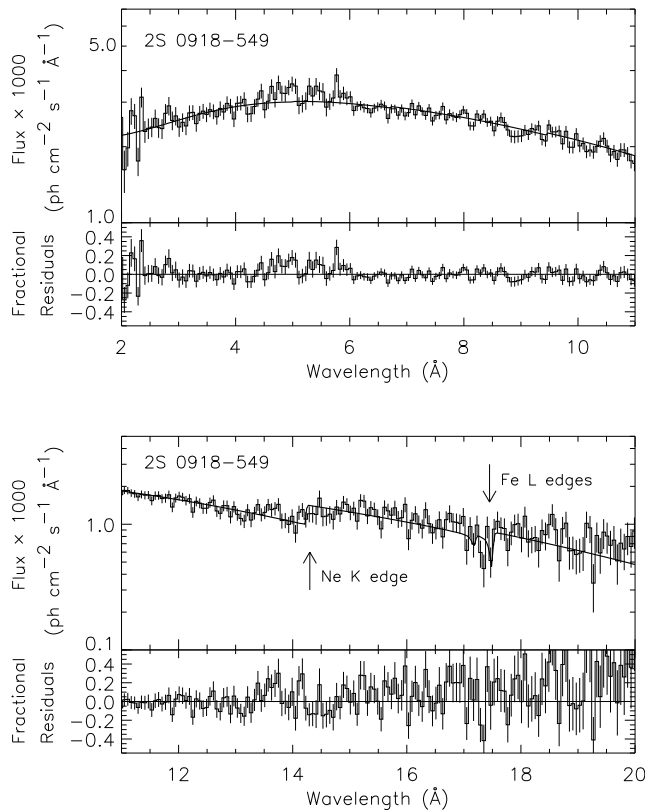


FIG. 1.— (upper panels) *Chandra* MEG first order spectrum of 2S 0918–549 with best-fit power-law + blackbody model including the O, Fe, and Ne edge models. For clarity, the data is binned to 0.06 Å. (lower panels) Fractional residuals ([data–model]/model) of the MEG first order spectral fit shown above. There are no features detected which are consistent with narrow emission or absorption lines. The arrows mark the Ne-K and Fe-L absorption edges at 14.3 and 17.5 Å respectively.

5340 and 7460  $\text{km s}^{-1}$  for the Ne X and O VIII lines fit by single Gaussians, we investigated how the EW limit changes as the model FWHM is increased. Increasing the FWHM of the line to 5000 (7000)  $\text{km s}^{-1}$ , increases

the EW upper limits by a factor of 1.5 (2.0).

To determine the best-fit continuum model for the *XMM* spectra of 2S 0918–549, we simultaneously fit the pn, MOS 2, and both RGS spectra. Since the pn timing mode response is not well calibrated below 1 keV, we only fit the pn spectrum in the 1.0–12.0 keV range. The energy range used for the MOS 2 was 0.3–8.0 keV and for the two RGS spectra it was 0.35–2.0 keV. We again fit both an absorbed power-law and an absorbed power-law + blackbody model. We also included a multiplicative constant to account for any instrumental normalization differences. During the *XMM* observation, the blackbody component was not significantly detected and we choose an absorbed power-law as the appropriate continuum model. The best-fit parameter values for the *XMM* spectral fit are given in Table 1.

For the high-resolution measurements of the absorption edge depths, we fit only the 2 RGS spectra using a power-law as the continuum model. Since the RGS covers only a limited wavelength range, 6.2–37.6 Å, we froze the power-law index to the best-fit value of the continuum model fit. Again we used the variable absorption model with O, Fe and Ne abundances set to zero, and included the appropriate edge models for O, Fe, and Ne. A Gaussian model was used to model the atomic O absorption line. The best-fit results are given in Tables 1 and 2 and shown in Figure 2. From the fits of the *XMM* RGS spectra, we find a Ne column density of  $N_{\text{Ne}} = (9.1 \pm 0.6) \times 10^{17} \text{ cm}^{-2}$  and an O column density of  $N_{\text{O}} = (1.96 \pm 0.07) \times 10^{18} \text{ cm}^{-2}$ , both consistent with the *Chandra* measurements. We find a Ne/O number ratio of  $0.46 \pm 0.03$ . The best-fit atomic O absorption line had a wavelength of  $23.504 \pm 0.013$  Å and an EW of  $0.020 \pm 0.005$  Å. The initial best-fit Fe-L column density left large residuals around the edge shape suggesting that the value was too large. It is possible that fits of the entire RGS wavelength range are not as sensitive to the Fe-L complex. To determine the correct Fe column, we fit only the 16.5–18 Å range with a simple model consisting of a power-law and the Fe-L table model. The power-law index was allowed to vary for this fit. From this fit, we found a Fe column of  $(8 \pm 3) \times 10^{16} \text{ cm}^{-2}$ , which was a much better visual match and consistent

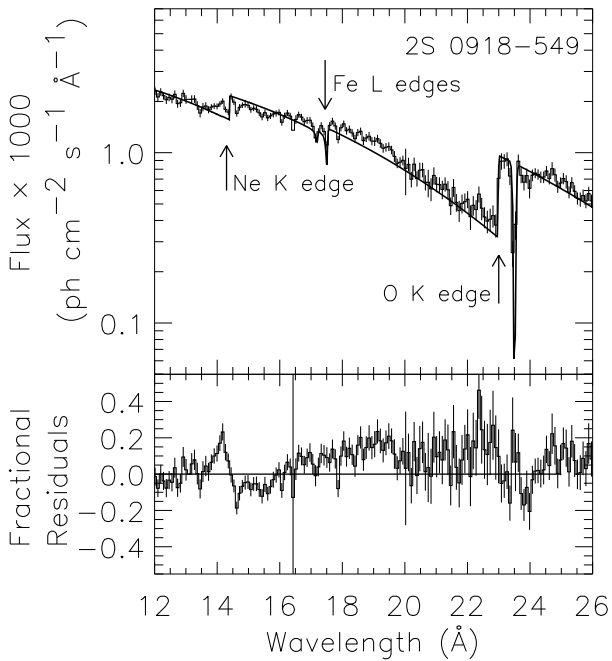


FIG. 2.— (upper panel) *XMM* combined RGS first order spectrum of 2S 0918–549 with best-fit power-law model including the O, Fe, and Ne edge models. For clarity, the data is binned to  $0.09 \text{ \AA}$ . (lower panel) Fractional residuals ( $[\text{data} - \text{model}] / \text{model}$ ) of the RGS first order spectral fit shown above. The absorption line at  $23.5 \text{ \AA}$  is the expected atomic O line. There are no other features detected which are consistent with narrow emission or absorption lines. The arrows mark the Ne-K, Fe-L and O-K absorption edges at  $14.3$ ,  $17.5$ , and  $23 \text{ \AA}$  respectively.

with the *Chandra* value. Our values for other parameters were determined with the Fe column density fixed to the above value.

We also searched for line features in the *XMM* spectrum of 2S 0918–549 using the same procedure as for the *Chandra* spectra. Gaussian models with fixed  $\text{FWHM} = 2000 \text{ km s}^{-1}$  were fit at each point in the wavelength range  $6.25$ – $37.6 \text{ \AA}$  for both RGS spectra. We place a  $3\sigma$  upper limit of  $0.05 \text{ \AA}$  on the EW of any line feature in the *XMM* spectrum of 2S 0918–549 in the wavelength range  $6$ – $18 \text{ \AA}$ . At larger wavelengths, the EW limit increases to  $0.6 \text{ \AA}$  at  $35 \text{ \AA}$ . Again, these EW limits are much lower than found in the 4U 1626–67 spectrum. If the FWHM of the Gaussian is increased to  $5000 \text{ km s}^{-1}$ , then the EW limit increases by roughly a factor of 2. There are residuals in the fit around  $14 \text{ \AA}$  and  $19 \text{ \AA}$  at the 20% level (see, Figure 2). The residuals of the 4U 1543–624 RGS spectral fit are similar (see, Figure 5), while the *Chandra* fit of 2S 0918–549 does not show the same features (see, Figure 1). This suggests that the residuals are due to remaining uncertainty in the instrument calibration.

The absorbed 2–10 keV flux of 2S 0918–549 was  $8.1 \times 10^{-11}$  and  $1.1 \times 10^{-10} \text{ erg cm}^{-2} \text{ s}^{-1}$  for the *Chandra* and *XMM* observations, respectively. This is an order of magnitude lower than the *ASCA* observation in 1995. The *Chandra* and *XMM* flux measurements are, however, consistent with other past observations, including

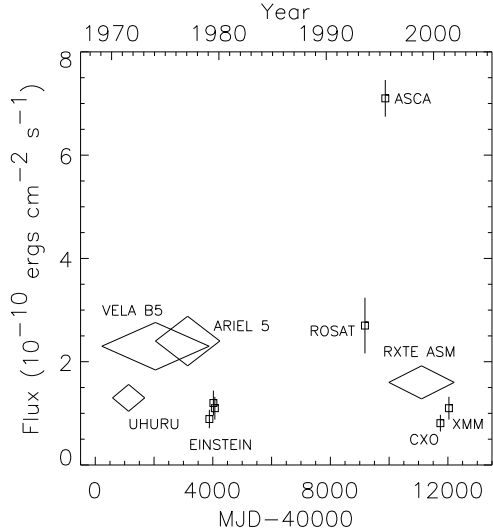


FIG. 3.— The 2–10 keV absorbed flux of 2S 0918–549 in units of  $10^{-10} \text{ ergs cm}^{-2} \text{ s}^{-1}$  over the past 30 years. The majority of the observations are reasonably consistent, except for the 1995 *ASCA* observation, when the source seems to have been in a bright state. The large diamonds represent average flux measurements for monitoring missions, while the small squares represent pointed observations.

the *RXTE* ASM flux measurements made contemporaneously (see, Figure 3). The spectral shape of the source has been roughly constant over the past 20 years, excluding the addition of a blackbody component in some more recent data. Although there is some difference in the best-fit slope of the power-law in each observation ( $\Gamma = 1.73$  for *ASCA*,  $2.04$  for *Chandra*, and  $2.265$  for *XMM*), this difference is not enough to account for the observed change in flux. Rather, the source seems to be brighter during the *ASCA* observation with larger normalizations measured for both the power-law and blackbody components. We suggest that 2S 0918–549 was in a bright state during the *ASCA* observation, similar to outbursts seen in other LMXBs (e.g., Homan & van der Klis 2000). As seen in X-ray color-color diagrams for sources in outburst, the hard color varies between outburst and quiescent phases while the soft color remains roughly the same (see, Muno et al. 2002). *ASCA*, *Chandra* and *XMM* have energy sensitivity which cover only the soft color energy range in standard color-color diagrams, so a spectral difference during an outburst may not be measurable with these instruments.

### 3.2. 4U 1543–624

We fit the four (+1 and -1; MEG and HEG) *Chandra* spectra of 4U 1543–624 jointly with both an absorbed power-law and an absorbed power-law + blackbody model in the wavelength range  $1.7$ – $25 \text{ \AA}$  for the MEG and  $1.3$ – $13 \text{ \AA}$  for the HEG. The pileup kernel in ISIS was used to model the pileup in the grating spectra. In addition, an edge model at  $43.7 \text{ \AA}$  was included to account for the instrumental C edge. We calculated that the appropriate optical depth for the instrumental C edge at the time of the 4U 1543–624 observation was 0.85. This edge is included in all *Chandra* spectral fits

of 4U 1543–624. The absorbed power-law + blackbody model was a significantly better fit to the data and we take this as the appropriate continuum model. The absorbed 2–10 keV flux of 4U 1543–624 during the *Chandra* observation was  $7.1 \times 10^{-10}$  erg cm $^{-2}$  s $^{-1}$ , which is consistent with past observations.

As was done with the 2S 0918–549 observations, we modeled the O and Ne edges with edge models and the Fe-L edge with the table model based on the latest cross-section from Kortright & Kim (2000). A Gaussian model was included to fit the atomic O absorption line at 23.5 Å. Since the most interesting features in the spectrum are at  $> 12$  Å, where pileup is no longer a problem, we fit the MEG spectra in the wavelength range 12–25 Å without the pileup kernel to measure the edge features. Pileup in the grating spectra enhances the instrumental residuals found at 2 keV, inflating the chi-squared value of the fit. By fitting only the high wavelength end of the spectra, we determine a more characteristic chi-squared value which can be used to judge the goodness of the fit. The blackbody component is only prominent at low wavelengths, so we chose to model the continuum in this limited wavelength range as a power-law. We found that if the equivalent hydrogen column density of the absorption model and the power-law index are allowed to vary, there is a degeneracy between the parameters that drives  $N_{\text{H}}$  and  $\Gamma$  to higher values. To remove this degeneracy, we fixed the photon index to that found in a continuum fit with the full model. The results can be found in Table 2.

From the absorption edge depths, we find a Ne column density of  $N_{\text{Ne}} = (12.4 \pm 1.1) \times 10^{17}$  cm $^{-2}$  and an O column density of  $N_{\text{O}} = (8.5 \pm 1.4) \times 10^{17}$  cm $^{-2}$ . The equivalent hydrogen column implied by the Ne edge is more than eight times that calculated from the O edge. We find a Ne/O number ratio of  $1.5 \pm 0.3$ , compared to the ISM ratio of 0.18. The atomic O absorption line was found at  $23.504 \pm 0.015$  Å with an EW of  $0.04 \pm 0.02$  Å. The measured Fe column is  $N_{\text{Fe}} = (3 \pm 2) \times 10^{16}$  cm $^{-2}$ .

As can be seen in Figure 4, no emission or absorption lines are apparent in the spectrum of 4U 1543–624. We performed a careful search of the *Chandra* spectral residuals to place limits on the presence of any spectral features in the 12–25 Å wavelength range of the MEG. Gaussian models with fixed FWHM=2000 km s $^{-1}$  were fit at each point. From this, we can place a  $3\sigma$  upper limit on the EW of any line feature, either emission or absorption. The EW limit increases with wavelength, varying from 0.02 Å at 12 Å to 1.0 Å at 23 Å, while broader line models give EW upper limits a factor of 2 larger. The EW limits found for the *Chandra* spectrum of 4U 1543–624 are lower than the emission line EWs found in the spectrum of 4U 1626–67. There have been a number of reports of a Fe K line detection in the spectrum of 4U 1543–624. There is no apparent line in the Fe K emission region (6.4–6.7 keV) of the *Chandra* spectrum. To place a limit on the EW of such a line, we fit an absorbed power-law + blackbody + Gaussian model to the full spectrum with a fixed line energy of 6.4 keV. The upper limit on the EW of the line is 60 eV.

The analysis of the *XMM* spectra of 4U 1543–624 is similar to the *XMM* analysis of 2S 0918–549. We first jointly fit the EPIC-pn, MOS 2, and RGS spectra with

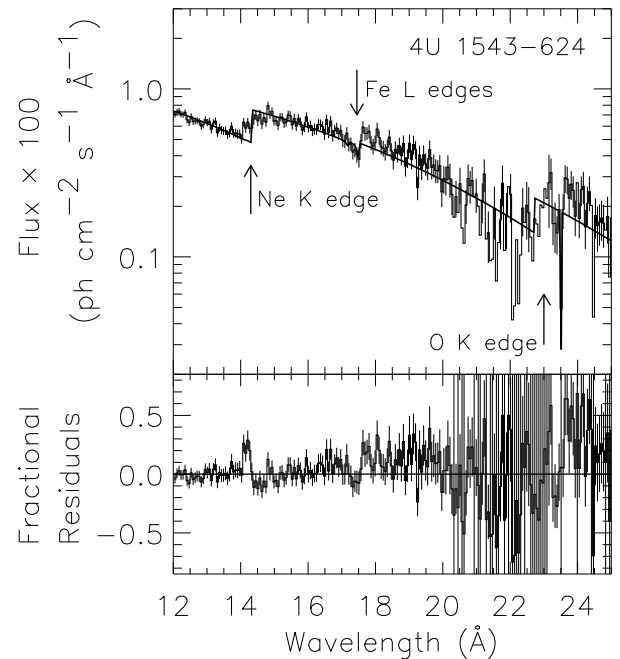


FIG. 4.— (upper panel) *Chandra* combined MEG first order spectrum of 4U 1543–624 with best-fit power-law model including the O, Fe, and Ne edge models. For clarity, the data is binned to 0.06 Å. (lower panel) Fractional residuals ([data–model]/model) of the MEG first order spectral fit shown above. The absorption line at 23.5 Å is the expected atomic O line. There are no other features detected which are consistent with narrow emission or absorption lines. The arrows mark the Ne-K, Fe-L and O-K absorption edges at 14.3, 17.5, and 23 Å respectively.

both an absorbed power-law and an absorbed power-law + blackbody. For 4U 1543–624, the power-law + blackbody was the best-fit continuum model. During the *XMM* observation, the absorbed 2–10 keV flux was  $4.2 \times 10^{-10}$  erg cm $^{-2}$  s $^{-1}$  which at the lower end of the range of observed flux of the source. The best-fit parameters of the *XMM* spectral fit of 4U 1543–624 has a steeper power-law photon index than found in the *Chandra* observation of the source. In addition, the blackbody temperature and normalization are different, although this difference could be due to incorrectly accounting for the absorption features. If the full *Chandra* spectrum is fit with a model that allows for a non-ISM Ne/O ratio, the blackbody temperature and normalization become consistent with the *XMM* result, which itself is consistent with previous results (see, e.g., Schultz 2002).

We added a Gaussian feature centered at 6.4 keV to the continuum model and determined the best fit width and flux of the line. We find that a wide, FWHM=2.64±0.14 keV, is allowed with a best-fit EW of  $370 \pm 40$  eV. This line is comparable to that found by Schultz (2002) in the *RXTE* data of 4U 1543–624. If the energy of the Gaussian is allowed to vary, the Gaussian model becomes even wider, FWHM≈6 keV, with a central energy of 4 keV. While it is interesting to note that both the *XMM* and *RXTE* data shows this similar feature, the large width and instability of the *XMM* fits, leads us to believe that the feature is not a detection of

Fe line emission.

For the high-resolution measurements of the absorption edge depths, we fit only the 2 RGS spectra using a power-law + blackbody as the continuum model. We froze both the power-law index and the blackbody temperature during the fits. Again we used the variable absorption model with O, Fe and Ne abundances set to zero, and included the appropriate edge models for O, Fe, and Ne. A Gaussian model was used to model the atomic O absorption line and another was included to fit a line feature at 23.36 Å which has been attributed to absorption by O in metallic compounds (i.e. oxides; e.g., Schulz et al. 2002) but is also consistent with the O II 1s-2p transition (see, Juett et al. 2003). We also found that the O edge could be better fit by including 2 edge models. The best-fit O edge wavelength is dependent on the form of the O (atomic vs. metallic compounds) and the presence of multiple forms of O would produce multiple edges.

The best-fit results are given in Tables 1 and 2 and shown in Figure 2. From the fits of the *XMM* RGS spectra of 4U 1543–624, we find  $N_{\text{Ne}} = (8.0 \pm 0.3) \times 10^{17} \text{ cm}^{-2}$  and  $N_{\text{Fe}} = (4.7 \pm 0.6) \times 10^{16} \text{ cm}^{-2}$ . For a single O edge, the best-fit wavelength is  $23.12 \pm 0.04$  Å with a column density of  $N_{\text{O}} = (14.8 \pm 0.2) \times 10^{17} \text{ cm}^{-2}$ . Fitting with two O edges yields wavelengths of  $22.86 \pm 0.04$  Å and  $23.19 \pm 0.03$  Å and column densities of  $(8.2 \pm 0.3) \times 10^{17} \text{ cm}^{-2}$  and  $(6.5 \pm 0.3) \times 10^{17} \text{ cm}^{-2}$ . The lower wavelength is consistent with the predicted O edge for atomic O while the higher wavelengths is expected from O bound in molecules. We find a Ne/O number ratio of  $0.54 \pm 0.03$ . For the atomic O absorption line, we find a best-fit wavelength  $23.515 \pm 0.006$  Å and an EW of  $0.0095 \pm 0.0011$  Å. The other line has a wavelength of  $23.371 \pm 0.009$  Å and an EW of  $0.0083 \pm 0.0014$  Å. Only the Fe-L column density is consistent between the *Chandra* and *XMM* observations. The *XMM* spectral analysis shows an increase in the O column density by a factor of 1.7, relative to the *Chandra* result, and a reduction by 60% in the Ne column density. While smaller than found in the *Chandra* spectrum, the Ne/O ratio of 0.54 is still significantly larger than the ISM value of 0.18.

We also searched for line features in the *XMM* spectrum of 4U 1543–624 using the same procedure as for the *Chandra* spectra. Gaussian models with fixed  $\text{FWHM} = 2000 \text{ km s}^{-1}$  were fit at each point in the wavelength range 6.2–35 Å for both RGS spectra. We place a  $3\sigma$  upper limit of 0.02 Å on the EW of any line feature in the *XMM* spectrum of 4U 1543–624 in the wavelength range 6–18 Å. At larger wavelengths, the EW limit increases to 0.3 Å at 35 Å. These EW limits are much lower than found in the 4U 1626–67 spectrum. When the  $\text{FWHM} = 5000 \text{ km s}^{-1}$ , the EW limits are a factor of 2 greater. As mentioned earlier, there are definite residuals in the spectral fit of 4U 1543–624 (see, Figure 5). We attribute these residuals to instrumental calibration uncertainty.

### 3.3. Residual Features

We now address the residuals found in our spectral analysis. For the *XMM* spectra of both sources, there are broad residual features at the 10–20% level. These residuals are consistent with the uncertainty in the cali-

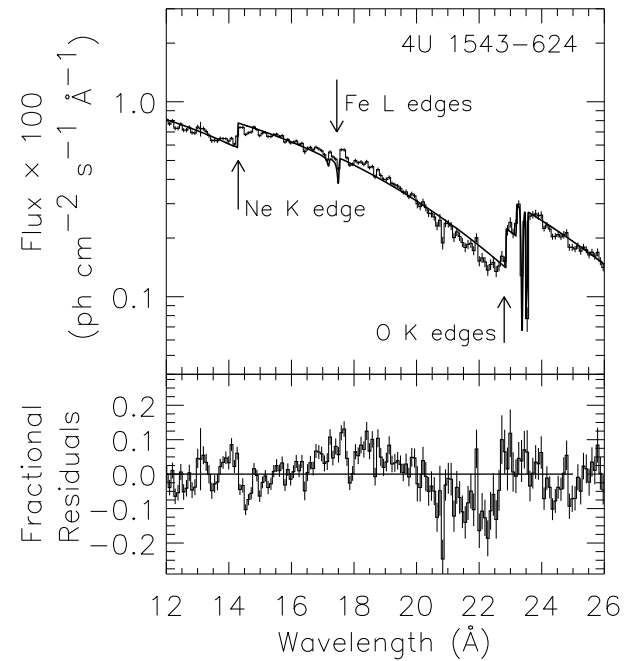


FIG. 5.— (upper panel) *XMM* combined RGS first order spectrum of 4U 1543–624 with best-fit power-law + blackbody model including the O, Fe, and Ne edge models. For clarity, the data is binned to 0.09 Å. (lower panel) Fractional residuals [(data–model)/model] of the RGS first order spectral fit shown above. The absorption line at 23.5 Å is the expected atomic O line while the line at 23.37 Å is consistent with O absorption in molecular compounds. There are no other features detected which are consistent with narrow emission or absorption lines. The arrows mark the Ne-K, Fe-L and O-K absorption edges at 14.3, 17.5, and 23 Å respectively.

bration of the RGS<sup>6</sup>. All spectra show some level of structure around the neutral Ne-K edge at 14.3 Å. For both instruments, the RGS and HETG, the interpretation of this feature is complicated by instrumental features at the same wavelength: the RGS has lost one of the CCDs that covered the 10.5–14.0 Å wavelength range reducing the effective area in this range, while the HETG nominal pointing places a chip gap in the –1 MEG order at the Ne-K edge.

While we do not claim a significant detection of any feature, the similar structure seen in all spectra suggest that the simple interpretation of a neutral Ne-K edge may not be entirely correct. Below we detail some possible astrophysical origins, remembering that instrumental effects are likely also important.

One explanation is that the feature is an emission line or a radiative recombination continuum (RRC) emission feature. At 14.0–14.3 Å, emission from a number of different ionization states of Fe is possible, but we would expect to see multiple features (e.g., as in the spectrum of Cyg X-1; Schulz et al. 2002). The O VIII RRC feature is also consistent with a 14.2 Å position. Again though, the lack of other O VIII emission features, in particular the O VIII emission line at 18.97 Å, makes this possibility

<sup>6</sup> See document XMM-SOC-CAL-TN-0030 available at [http://xmm.vilspa.esa.es/external/xmm\\_sw/cal/calib/index.shtml](http://xmm.vilspa.esa.es/external/xmm_sw/cal/calib/index.shtml)

TABLE 2. PHOTOELECTRIC ABSORPTION EDGE MEASUREMENTS<sup>a</sup>

Edge	$\lambda$ (Å)	Optical depth $\tau$	$N_Z$ ( $10^{17}$ cm $^{-2}$ )	$N_H$ ( $10^{21}$ cm $^{-2}$ )
2S 0918–549: <i>Chandra</i> result				
O K	$23.0 \pm 0.3$	$1.08 \pm 0.18$	$19 \pm 3$	$3.9 \pm 0.6$
Fe L III	$17.49 \pm 0.02^b$	$0.7 \pm 0.4$	$1.0 \pm 0.6$	$3.7 \pm 2.2$
Ne K	$14.24^{+0.2}_{-0.02}$	$0.36 \pm 0.06$	$9.9 \pm 1.7$	$11.4 \pm 1.9$
2S 0918–549: <i>XMM</i> result				
O K	$22.99 \pm 0.08$	$1.11 \pm 0.04$	$19.6 \pm 0.7$	$4.00 \pm 0.14$
Fe L III	$17.50 \pm 0.03^b$	$0.6 \pm 0.2$	$0.08 \pm 0.03$	$3.0 \pm 1.1$
Ne K	$14.40 \pm 0.03$	$0.33 \pm 0.02$	$9.1 \pm 0.6$	$10.4 \pm 0.6$
4U 1543–624: <i>Chandra</i> result				
O K	$22.72^{+0.05}_{-0.03}$	$0.48 \pm 0.08$	$8.5 \pm 1.4$	$1.7 \pm 0.3$
Fe L III	$17.49 \pm 0.04^b$	$0.21 \pm 0.14$	$0.3 \pm 0.2$	$1.1 \pm 0.7$
Ne K	$14.330 \pm 0.017$	$0.45 \pm 0.04$	$12.4 \pm 1.1$	$14.2 \pm 1.3$
4U 1543–624: <i>XMM</i> result				
O K	$22.86 \pm 0.04$	$0.64 \pm 0.016$	$8.2 \pm 0.3$	$1.67 \pm 0.06$
O K	$23.19 \pm 0.03$	$0.368 \pm 0.016$	$6.5 \pm 0.3$	$1.32 \pm 0.06$
Fe L III	$17.50 \pm 0.02^b$	$0.33 \pm 0.04$	$0.47 \pm 0.06$	$1.7 \pm 0.2$
Ne K	$14.286^{+0.012}_{-0.05}$	$0.291 \pm 0.010$	$8.0 \pm 0.3$	$9.2 \pm 0.3$

<sup>a</sup>All errors are quoted at the 90%-confidence level. Atomic cross-sections taken from Henke et al. (1993) for O and Ne, and Kortright & Kim (2000) for Fe-L. Interstellar abundances taken from Wilms et al. (2000).

<sup>b</sup>We define the absorption edge energy for Fe as the energy at which the edge structure reaches its minimum value.

less probable.

The O VIII absorption edge is also located at 14.2 Å and the *Chandra* spectrum of 4U 1543–624 (see, Figure 4) seems to suggest that 2 edges, one at Ne-K and another at O VIII may be a plausible solution. Finally, the feature might be related to the Ne absorption edge. Unlike other elements, Ne cannot be in molecular forms which might cause structure at the K shell absorption edge. We can not rule out however unanticipated structure in the edge shape, in particular if the Ne-rich absorbing material has some velocity, we might expect to find a velocity shifted edge structure. The interpretation of this feature is hampered by the lack of high-resolution atomic data on X-ray absorption edges. As we acquire more data on X-ray absorption edges, it will become possible to determine if this structure is “normal” or instead suggests the presence of more interesting phenomena.

#### 4. DISCUSSION

We have shown that the *Chandra*/HETGS and *XMM*/RGS spectra of 2S 0918–549 and 4U 1543–624 are well fit by models that allow for absorption columns of neutral Ne and O with abundance ratios significantly different from the expected ISM ratio. The *Chandra* spectrum of 2S 0918–549 has a best fit Ne/O number ratio of  $0.52 \pm 0.12$ , or roughly  $3 \times$  the ISM value of 0.18. The *XMM* fit of 2S 0918–549 gives a consistent Ne/O number ratio of  $0.46 \pm 0.03$ . The best-fit model for the *Chandra* spectrum of 4U 1543–624 has a Ne/O number ratio of  $1.5 \pm 0.3$ , while the best-fit *XMM* model has a Ne/O number ratio of  $0.54 \pm 0.03$ . The unusual abundance ratios as well as the variability seen in the observations of 4U 1543–624 lead us to conclude that there is absorption local to these binaries and that the material is Ne enriched.

From the  $L_X/L_{\text{opt}}$  ratios of 2S 0918–549 and 4U 1543–624, we expect these binaries to have orbital periods  $\lesssim 60$  min based on the empirical relationship determined by van Paradijs & McClintock (1994).

We searched the *Chandra* lightcurves for orbital modulation, but found no modulations larger than 1–2%. *XMM* provided a more sensitive search for orbital modulations, but we found no signatures of orbital modulation at fractional rms upper limits of 0.14–0.3%. Confirmation of such short orbital periods would place 2S 0918–549 and 4U 1543–624 in the class of ultracompact LMXBs ( $P_{\text{orb}} \lesssim 80$  min). Ultracompact binaries require H-depleted or degenerate dwarf companions (Joss et al. 1978; Nelson et al. 1986). Such companions would be expected to have non-standard abundances compared to ISM values. The *Chandra* spectrum of 4U 1626–67 revealed absorption edges of C, O, and Ne which are 5 times larger than would be predicted given the hydrogen column density measured in the UV. For 4U 1626–67, the measured local abundance ratios, if the excess material is assumed to have originated around the binary, are consistent with the expected abundances in the chemically fractionated core of a C-O or O-Ne-Mg WD (Schulz et al. 2001). The evidence for Ne absorption in 2S 0918–549 and 4U 1543–624 hints at a similarity between these sources and 4U 1626–67. In addition, there is evidence that the optical spectra of this group of sources is also similar to 4U 1626–67 with no H or He lines detected, but with a C III/N III emission line near 4640 Å (Wang & Chakrabarty 2003, in preparation). Based on the similarity between these sources and 4U 1626–67, we previously attributed the excess Ne absorption in 2S 0918–549 and 4U 1543–624 to material local to the sources, and suggested that these systems contained a Ne-rich degenerate donor (Juett et al. 2001).

The one assumption we have made in this analysis is that the absorption is from neutral material only. If there is a sizable contribution to the absorption from material local to the binary, this assumption is most likely not valid, since we would expect ionization of the local material from the central source. Accounting for ionization of the material may explain the large Ne/O ratios observed. We find Ne/O ratios larger than the 0.22 in-

ferred for the local absorption in the *Chandra* spectrum of 4U 1626–67 (Schulz et al. 2001). Ne/O ratios for local absorption in our source will be even higher than the measured total line-of-sight ratio once ISM contributions are removed, since the O column from the ISM should be larger than the Ne column. Unfortunately, we can not do this calculation, as was possible for 4U 1626–67, since we do not know the expected ISM contribution for 2S 0918–549 or 4U 1543–624. If the local material is affected by ionization, the effect will be different for each element. O will become ionized before Ne, leading to an enhanced Ne/O ratio as measured by the neutral edges. While it is tempting to assume that ionization is the only cause for the unusual abundances, we point out that if the local material was of standard abundances, we would expect local absorption from higher Z elements, like Mg and Si, which are not seen in the spectra of 2S 0918–549 or 4U 1543–624. This leads us to conclude that material must have some enhancement of Ne to show such strong absorption.

One of the most interesting results is the difference in the Ne and O column densities in the two observations of 4U 1543–624. The *XMM* results show a increase in the O column density with a decrease in the Ne column density. In addition, the *XMM* spectrum is both softer and has a lower luminosity in the 2–10 keV band than the *Chandra* spectrum, which suggests that the source was not in the same state in the *Chandra* and *XMM* observations. We suggest that the difference in the 4U 1543–624 results provides support for the local nature of the absorption. Since the high-resolution results of 2S 0918–549 are consistent not only in the measured Ne/O number ratio but also in the spectral model in general, we are confident that instrumental differences do not have a significant effect on the spectral results. It is interesting to note the the Ne/O ratios found in the *Chandra* and *XMM* observations of 2S 0918–549 are smaller than the inferred value from the *ASCA* result of Juett et al. (2001), while at the same time the flux of 2S 0918–549 has decreased by a factor of 10 since the *ASCA* observation. It is possible that the state changes alter the ionization structure of the local material, which in turn changes the absorbing columns of neutral Ne and O. It will be difficult to separate the effect of unusual abundances from ionization changes without more data on these sources. We propose that multiple observations of 4U 1543–624 using simultaneous high-resolution and broadband observations will probe the connection between spectral state differences and the column density variations. It is important to note that ionization effects and the ISM contribution must be understood before it is possible to determine the intrinsic Ne/O abundance ratio of the local material, which can then be used to place constraints on the composition of the companion.

Although we attribute the excess Ne absorption in 2S 0918–549 and 4U 1543–624 to local material in both of the binaries, we also consider the possibility that the excess Ne is due to enhancements of the ISM along the line of sight. The best measurement of absorption toward an X-ray binary, the *Chandra* spectral analysis of Cyg X-1, shows columns of O and Ne that are consistent with standard ISM abundances (Schulz et al. 2002). To quantify the variations of the ISM abundances, we have undertaken a study of the ISM using column density

measurements from the spectra of X-ray binaries (Juett et al. 2003). Initial results show that other LMXBs do not show the Ne/O ratios measured for these sources. At most, Ne/O number ratios are only twice the expected ISM values. This is still significantly smaller than we find in 2S 0918–549 and 4U 1543–624, but does suggest that there are some variations between lines-of-sight. We still favor the interpretation that there is absorbing material local to the binaries, and that this is strengthened by the observation-to-observation variations in the Ne/O number ratio of 4U 1543–624 which could not be due to the ISM.

Analysis of the *Chandra* and *XMM* spectra of 2S 0918–549 and 4U 1543–624 found no Ne or O lines like those seen in 4U 1626–67. The absence of strong lines in the spectra of 2S 0918–549 and 4U 1543–624 demonstrates that their circumbinary environments are different compared to 4U 1626–67. One possible reason for this difference may be that 4U 1626–67 is a pulsar with  $B=3 \times 10^{12}$  G (Orlandini et al. 1998), while 2S 0918–549 and 4U 1543–624 are likely to have weak magnetic fields ( $\sim 10^8$  G). This undoubtedly results in a substantial difference in the accretion flow geometry. There is weak evidence for a line-like feature at 6.4 keV in the *XMM* spectrum of 4U 1543–624. This feature is very broad and could possibly be due to a mis-modeling of the continuum emission rather than a Fe line. In addition, there is evidence for structure around the Ne edge in the spectra of both sources. It is likely that this is due to instrumental effects but could also be due to structure in either neutral Ne edges or possibly due to confusion with ionized O edges.

Recent *RXTE* and *BeppoSAX* observations of 2S 0918–549 found the first thermonuclear X-ray bursts from this source (Jonker et al. 2001; Cornelisse et al. 2002). Both bursts were short, with durations  $\lesssim 100$  s. These short bursts suggest that H and/or He is undergoing unstable burning on the surface of the NS. If the companion has a large C abundance, we might expect to see a much longer burst ( $\approx 1$  hr), like the “superbursts” seen in some LMXBs, which have been attributed to thermonuclear burning of C on neutron star surfaces (Cornelisse et al. 2000; Cumming & Bildsten 2001; Strohmayer & Brown 2001). The more ordinary properties of the X-ray bursts from 2S 0918–549 may indicate that the donor is not a C-O dwarf as suggested for 4U 1626–67. In this case, another mechanism for Ne enhancement is needed. On the other hand, it may still be possible for a carbon accretor to show short X-ray bursts. One possibility is that while the companion is H-deficient, there is still a non-negligible H fraction that is accreted by the NS and is then responsible for the Type I X-ray bursts (e.g., Nelson et al. 1986). Alternatively, the heavy elements (C, O, and Ne) may undergo spallation during accretion, leaving He and H nuclei which could then undergo unstable thermonuclear burning in the usual way (Bildsten, Salpeter, & Wasserman 1992). Spallation reactions would produce  $\gamma$ -ray emission lines at 4.4 and 6.1 MeV. Unfortunately, the strength of these lines as calculated by Bildsten et al. (1992) is below current observational detection limits. For a 1 Ms observation with *Integral*, the detection sensitivities are  $\sim 1000$  times higher than the most optimistic line flux estimates.

We would like to thank the anonymous referee for his comments which greatly improved this paper. For help in determining the optical position of 2S 0918–549, we thank Zhongxiang Wang. We are grateful to the HETGS instrument team at MIT for their help and advice in analyzing these data. We especially thank John Davis for assistance in analyzing piled-up grating data, John Houck for his help with and modifications of ISIS, and

Herman Marshall for information on the ACIS calibration status and the appropriate QE correction table. We also acknowledge useful discussions with Lars Bildsten, Andrew Cumming, Duncan Galloway, Peter Jonker, Eric Kuulkers, Jon Miller, Mike Muno, Eric Pfahl, Dimitrios Psaltis, and Norbert Schulz. This work was supported in part by NASA under contracts NAS8-38249 and NAS8-01129 and grant NAG5-9184.

## REFERENCES

Angelini, L., White, N. E., Nagase, F., Kallman, T. R., Yoshida, A., Takeshima, T., Becker, C., & Paerels, F. 1995, ApJ, 449, L41

Asai, K., Dotani, T., Nagase, F., Mitsuda, K. 2000, ApJS, 131, 571

Arnaud, K. A. 1996, in *Astronomical Data Analysis Software and Systems V*, ed. G. Jacoby & J. Barnes (San Francisco: ASP Conf. Ser. 101), 17

Bildsten, L., Salpeter, E. E., & Wasserman, I. 1992, ApJ, 384, 143

Bradt, H. V. D. & McClintock, J. E. 1983, ARA&A, 21, 13

Chevalier, C. & Ilovaisky, S. A. 1987, A&A, 172, 167

Christian, D. J., & Swank, J. H. 1997, ApJS, 109, 177

Christian, D. J., White, N. E., & Swank, J. H. 1994, ApJ, 422, 791

Cornelisse, R., Heise, J., Kuulkers, E., Verbunt, F., & in't Zand, J. J. M. 2000, ApJ, 535, L21

Cornelisse, R., et al. 2002, A&A, 392, 885

Cumming, A. & Bildsten, L. 2001, ApJ, 559, L127

Davis, J. E. 2003, in *Astronomical Telescopes and Instrumentation 2002*, ed. J. Truemper, & H. Tananbaum, SPIE Conf. Proc., 4851, 101

den Herder, J. W., et al. 2001, A&A, 365, L7

Farinelli, R. et al. 2003, A&A, 402, 1021

Forman, W. et al. 1978, ApJS, 38, 357

Galloway, D. K., Chakrabarty, D., Morgan, E. H., & Remillard, R. A. 2002, ApJ, 576, L137

Henke, B. L., Gullikson, E. M., & Davis, J. C. 1993, *Atomic Data & Nucl. Data Tables*, 54, 181

Homan, J. & van der Klis, M. 2000, ApJ, 539, 847

Homer, L., Charles, P. A., Naylor, T., van Paradijs, J., Aurère, M., & Koch-Miramond, L. 1996, MNRAS, 282, L37

Houck, J. C., & DeNicola, L. A. 2000, in *Astronomical Data Analysis Software and Systems IX*, ed. N. Manset, C. Veillet, & D. Crabtree (San Francisco: ASP Conf. Ser. 216), 591

Jonker, P. G. et al. 2001, ApJ, 553, 335

Joss, P. C., Avni, Y., & Rappaport, S. 1978, ApJ, 221, 645

Juett, A. M., Psaltis, D., & Chakrabarty, D. 2001, ApJ, 560, L59

Kortright, J. B., & Kim, S.-K. 2000, Phys. Rev. B, 62, 12216

Kuster, M. et al. 2002, in *New Visions of the X-ray Universe in the XMM-Newton and Chandra Era*, ed. F. Jansen, in press (astro-ph/0203207)

Markwardt, C. B., Swank, J. H., Strohmayer, T. E., in 't Zand, J. J. M., & Marshall, F. E. 2002, ApJ, 575, L21

Markwardt, C. B., Smith, E., & Swank, J. H. 2003, IAU Circ., 8080

Mason, K. O., et al. 2001, A&A, 365, L36

McClintock, J., Canizares, C., Hiltner, W. A., & Petro, L. 1978, IAU Circ., 3251

Middleditch, J., Mason, K. O., Nelson, J. E., & White, N. E. 1981, ApJ, 244, 1001

Monet, D. E. A., et al. 1998, *The USNO-A2.0 Catalog* (Washington, D. C.: U. S. Naval Observatory)

Muno, M. P., Remillard, R. A., & Chakrabarty, D. 2002, ApJ, 568, L35

Nelson, L. A., Rappaport, S. A., & Joss, P. C. 1986, ApJ, 304, 231

Orlandini, M., et al. 1998, ApJ, 500, L163

Paczynski, B., & Sienkiewicz, R. 1981, ApJ, 248, L27

Paerels, F., et al. 2001, ApJ, 546, 338

Plucinsky, P. P. et al. 2003, in *Astronomical Telescopes and Instrumentation 2002*, ed. J. Truemper, & H. Tananbaum, SPIE Conf. Proc., 4851, 89

Rappaport, S., Joss, P. C., & Webbink, R. F. 1982, ApJ, 254, 616

Schultz, J. 2002, A&A, 397, 249

Schulz, N. S. 1999, ApJ, 511, 304

Schulz, N. S., Chakrabarty, D., Marshall, H. L., Canizares, C. R., Lee, J. C., & Houck, J. 2001, ApJ, 563, 941

Schulz, N. S., Cui, W., Canizares, C. R., Marshall, H. L., Lee, J. C., Miller, J. M., & Lewin, W. H. G. 2002, ApJ, 565, 1141

Singh, K. P., Apparao, K. M. V., Kraft, R. P. 1994, ApJ, 421, 753

Smale, A. P., & Lochner, J. C. 1992, ApJ, 395, 582

Stella, L., Priedhorsky, W., & White, N. E. 1987, ApJ, 312, L17

Strohmayer, T. E. & Brown, E. F. 2002, ApJ, 566, 1045

Strüder, L., et al. 2001, A&A, 365, L18

Turner, M. J. L., et al. 2001, A&A, 365, L27

van Paradijs, J., & McClintock, J. E. 1994, A&A, 290, 133

Walter, F. M., et al. 1982, ApJ, 253, L67

Warner, B. 1995, Ap&SS, 225, 249

Warwick, R. S. et al. 1981, MNRAS, 197, 865

Weisskopf, M. C., Brinkman, B., Canizares, C., Garmire, G., Murray, S., & van Speybroeck, L. P. 2002, PASP, 114, 1

White, N. E., Kallman, T. R., & Angelini, L. 1997, in *X-Ray Imaging and Spectroscopy of Cosmic Hot Plasmas*, ed. F. Makino & K. Mitsuda (Tokyo: Universal Academy Press), 411

White, N. E., & Swank, J. H. 1982, ApJ, 253 L61

Wilms, J., Allen, A., & McCray, R. 2000, ApJ, 542, 914

Yungelson, L. R., Nelemans, G., & van den Heuvel, E. P. J. 2002, A&A, 388, 546